

Northumbria Research Link

Citation: Vo, Thuc and Lee, Jaehong (2011) Free vibration of axially loaded thin-walled composite Timoshenko beams. *Archive of Applied Mechanics*, 81 (9). pp. 1165-1180. ISSN 0939-1533

Published by: Springer

URL: <http://dx.doi.org/10.1007/s00419-010-0477-9>

This version was downloaded from Northumbria Research Link:
<http://nrl.northumbria.ac.uk/14091/>

Northumbria University has developed Northumbria Research Link (NRL) to enable users to access the University's research output. Copyright © and moral rights for items on NRL are retained by the individual author(s) and/or other copyright owners. Single copies of full items can be reproduced, displayed or performed, and given to third parties in any format or medium for personal research or study, educational, or not-for-profit purposes without prior permission or charge, provided the authors, title and full bibliographic details are given, as well as a hyperlink and/or URL to the original metadata page. The content must not be changed in any way. Full items must not be sold commercially in any format or medium without formal permission of the copyright holder. The full policy is available online: <http://nrl.northumbria.ac.uk/policies.html>

This document may differ from the final, published version of the research and has been made available online in accordance with publisher policies. To read and/or cite from the published version of the research, please visit the publisher's website (a subscription may be required.)

www.northumbria.ac.uk/nrl



1 Free vibration of axially loaded thin-walled composite Timoshenko beams

2 Thuc Phuong Vo* and Jaehong Lee†

3 *Department of Architectural Engineering, Sejong University*
4 *98 Kunja Dong, Kwangjin Ku, Seoul 143-747, Korea*

5 (Dated: October 19, 2013)

Based on shear-deformable beam theory, free vibration of thin-walled composite Timoshenko beams with arbitrary lay-ups under a constant axial force is presented. This model accounts for all the structural coupling coming from material anisotropy. Governing equations for flexural-torsional-shearing coupled vibrations are derived from Hamilton's principle. The resulting coupling is referred to as sixfold coupled vibrations. A displacement-based one-dimensional finite element model is developed to solve the problem. Numerical results are obtained for thin-walled composite beams to investigate the effects of shear deformation, axial force, fiber angle, modulus ratio on the natural frequencies, corresponding vibration mode shapes and load-frequency interaction curves.

6 **Keywords:** Thin-walled composite Timoshenko beams; shear deformation; sixfold coupled vibrations; axial force.

7 1. INTRODUCTION

8 Fiber-reinforced plastics have been used over the past few decades in a variety of structures. Composites have
9 many desirable characteristics, such as high ratio of stiffness and strength to weight, corrosion resistance and mag-
10 netic transparency. Thin-walled structural shapes made up of composite materials, which are usually produced by
11 pultrusion, are being increasingly used in many civil, mechanical and aerospace engineering applications. However, it
12 is well known that thin-walled composite structures might be under axial force when used in above applications and
13 are very susceptible to flexural-torsional buckling and display complex vibrational behavior. Therefore, the accurate
14 prediction of their stability limit state and dynamic characteristics is of the fundamental importance in the design of
15 composite structures.

16 The theory of thin-walled open-section members made of isotropic materials was first developed by Vlasov [?] and
17 Gjelsvik [?]. Since the early works of Bleich et al. [?] and Timoshenko et al. [?,?], the investigation into vibration
18 of thin-walled beams under axial loads of these members has been carried out extensively. A tensile axial load is

*Present Address: Department of Engineering, University of Liverpool, Brownlow Street, Liverpool L69 3GQ, UK

†Professor, corresponding author. Tel.:+82-2-3408-3287; fax:+82-2-3408-3331

; Electronic address: jhlee@sejong.ac.kr

19 well-known to increase the natural frequencies, whereas a compressive axial load will decrease the natural frequencies
20 of beam members. For thin-walled composite beams, with the presence of the additional coupling effects from material
21 anisotropy, these members under axial force exhibit strong coupling. Therefore, their vibration characteristic becomes
22 more complicated than isotropic material even for doubly symmetric cross-section. This problem has been studied
23 analytically by using some numerical techniques. The finite element method has been widely used because of its
24 versatility and **a large amount of work** was devoted **to obtain** the acceptable results. Bank and Kao [?] analyzed
25 free and forced vibration of thin-walled fibre reinforced composite material beams by using the Timoshenko beam
26 theory. Cortinez and Piovan [?] presented a theoretical model for the vibration and buckling analysis of thin-walled
27 composite beams. Later, Machado and Cortinez [?] investigated the influence of the initial in-plane deformations,
28 generated by the action of a static external loading, as well as the effect of shear flexibility on the dynamic behavior
29 of bisymmetric thin-walled composite beams. In their research [?,?], the analysis was based on a geometrically
30 non-linear theory and thin-walled composite beams for both open and closed cross-sections and the shear flexibility
31 (bending, non-uniform warping) were incorporated. However, it was strictly valid for symmetric balanced laminates
32 and especially orthotropic laminates. On the other hand, another effective method solving the dynamic problem of
33 thin-walled composite beams is to derive the exact stiffness matrices based on the solution of differential equations.
34 Most of those studies adopted an analytical method that required explicit expressions of exact displacement functions
35 for governing equations. By using this method, several authors have investigated the free vibration characteristic
36 of axially loaded thin-walled closed-section composite beams (Banerjee et al. [?-?] and Li et al.[?,?] and Kaya
37 and Ozgumus [?]) but only a few applied for thin-walled open-section composite beams. Kim et al.[?,?] evaluated
38 dynamic stiffness matrix for flexural-torsional, lateral buckling and free vibration analyses of mono-symmetric thin-
39 walled composite beams. A literature survey on the subject has revealed that studies of free vibration of thin-walled
40 composite Timoshenko beams with arbitrary lay-ups including the influences of axial force and shear deformation in a
41 unitary manner are limited. This complicated problem is not well-investigated and there is a need for further studies.

42 In this paper, which is an extension of the authors' previous works [?-?], free vibration of axially loaded thin-
43 walled composite Timoshenko beams with arbitrary lay-ups is presented. This model is based on the first-order
44 shear-deformable beam theory, and accounts for all the structural coupling coming from the material anisotropy.
45 The seven governing differential equations for flexural-torsional-shearing coupled vibrations are derived from the
46 Hamilton's principle. Numerical results are obtained for thin-walled composite beams to investigate the effects of
47 shear deformation, axial force, fiber angle, modulus ratio on the natural frequencies and corresponding vibration

48 mode shapes as well as load-frequency interaction curves.

49 2. KINEMATICS

50 The theoretical developments presented in this paper require two sets of coordinate systems which are mutually
 51 interrelated. The first coordinate system is the orthogonal Cartesian coordinate system (x, y, z) , for which the x and
 52 y axes lie in the plane of the cross section and the z axis parallel to the longitudinal axis of the beam. The second
 53 coordinate system is the local plate coordinate (n, s, z) as shown in Fig.??, wherein the n axis is normal to the middle
 54 surface of a plate element, the s axis is tangent to the middle surface and is directed along the contour line of the
 55 cross section. The (n, s, z) and (x, y, z) coordinate systems are related through an angle of orientation θ . As defined
 56 in Fig.?? a point P , called the pole, is placed at an arbitrary point x_p, y_p . A line through P parallel to the z axis is
 57 called the pole axis.

58 To derive the analytical model for a thin-walled composite beam, the following assumptions are made:

- 59 1. The contour of the thin wall does not deform in its own plane.
- 60 2. Transverse shear strains $\gamma_{xz}^\circ, \gamma_{yz}^\circ$ and warping shear γ_ω° are incorporated. It is assumed that they are uniform
 61 over the cross-sections.
- 62 3. Each laminate is thin and perfectly bonded.
- 63 4. Local buckling is not considered.

64 According to assumption 1, the midsurface displacement components \bar{u}, \bar{v} at a point A in the contour coordinate
 65 system can be expressed in terms of a displacements U, V of the pole P in the x, y directions, respectively, and the
 66 rotation angle Φ about the pole axis

$$\bar{u}(s, z) = U(z) \sin \theta(s) - V(z) \cos \theta(s) - \Phi(z)q(s) \quad (1a)$$

$$\bar{v}(s, z) = U(z) \cos \theta(s) + V(z) \sin \theta(s) + \Phi(z)r(s) \quad (1b)$$

67 These equations apply to the whole contour. For each element of middle surface, the midsurface shear strains in the
 68 contour can be expressed with respect to the transverse shear and warping shear strains.

$$\bar{\gamma}_{nz}(s, z) = \gamma_{xz}^\circ(z) \sin \theta(s) - \gamma_{yz}^\circ(z) \cos \theta(s) - \gamma_\omega^\circ(z)q(s) \quad (2a)$$

$$\bar{\gamma}_{sz}(s, z) = \gamma_{xz}^\circ(z) \cos \theta(s) + \gamma_{yz}^\circ(z) \sin \theta(s) + \gamma_\omega^\circ(z)r(s) \quad (2b)$$

69 Further, it is assumed that midsurface shear strain in $s - n$ direction is zero ($\bar{\gamma}_{sn} = 0$). From the definition of the
70 shear strain, $\bar{\gamma}_{sz} = 0$ can also be given for each element of middle surface as

$$\bar{\gamma}_{sz}(s, z) = \frac{\partial \bar{v}}{\partial z} + \frac{\partial \bar{w}}{\partial s} \quad (3)$$

71 **After substituting \bar{v} from Eq.(??) into Eq.(??)**, the out-of-plane shell displacement \bar{w} can be integrated with
72 respect to s from the origin to an arbitrary point on the contour

$$\bar{w}(s, z) = W(z) + \Psi_y(z)x(s) + \Psi_x(z)y(s) + \Psi_\omega(z)\omega(s) \quad (4)$$

73 where Ψ_x, Ψ_y and Ψ_ω represent rotations of the cross section with respect to x, y and ω , respectively, given by

$$\Psi_y = \gamma_{xz}^\circ(z) - U' \quad (5a)$$

$$\Psi_x = \gamma_{yz}^\circ(z) - V' \quad (5b)$$

$$\Psi_\omega = \gamma_\omega^\circ(z) - \Phi' \quad (5c)$$

74 When the transverse shear effect is ignored, Eq.(??) degenerates to $\Psi_y = -U'$, $\Psi_x = -V'$ and $\Psi_\omega = -\Phi'$. As a result,
75 the number of unknown variables reduces to four leading to the Euler-Bernoulli beam model. The prime ($'$) is used
76 to indicate differentiation with respect to z ; and ω is the so-called sectorial coordinate or warping function given by

$$\omega(s) = \int_{s_0}^s r(s)ds \quad (6)$$

77 The displacement components u, v, w representing the deformation of any generic point on the profile section are
78 given with respect to the midsurface displacements $\bar{u}, \bar{v}, \bar{w}$ by assuming the first order variation of inplane displacements
79 v, w through the thickness of the contour as

$$u(s, z, n) = \bar{u}(s, z) \quad (7a)$$

$$v(s, z, n) = \bar{v}(s, z) + n\bar{\psi}_s(s, z) \quad (7b)$$

$$w(s, z, n) = \bar{w}(s, z) + n\bar{\psi}_z(s, z) \quad (7c)$$

80 where, $\bar{\psi}_s$ and $\bar{\psi}_z$ denote the rotations of a transverse normal about the z and s axis, respectively. The function $\bar{\psi}_z$
81 can be determined by considering the shear strains γ_{nz} at midsurface

$$\gamma_{nz}(s, z) = \frac{\partial w}{\partial n} + \frac{\partial u}{\partial z} = \bar{\psi}_z + \frac{\partial \bar{u}}{\partial z} \quad (8)$$

82 By substituting Eqs.(??), (??) and (??) into Eq.(??), the function $\bar{\psi}_z$ can be written as

$$\bar{\psi}_z = \Psi_y \sin \theta - \Psi_x \cos \theta - \Psi_\omega q \quad (9)$$

83 Similarly, using the assumption that the shear strain γ_{sn} should vanish at midsurface, the function $\bar{\psi}_s$ can be obtained

$$\bar{\psi}_s = -\frac{\partial \bar{u}}{\partial s} \quad (10)$$

84 The non-zero strains associated with the small-displacement theory of elasticity are given by

$$\epsilon_z(s, z, n) = \frac{\partial w}{\partial z} = \bar{\epsilon}_z(s, z) + n\bar{\kappa}_z(s, z) \quad (11a)$$

$$\gamma_{sz}(s, z, n) = \frac{\partial w}{\partial s} + \frac{\partial v}{\partial z} = \bar{\gamma}_{sz}(s, z) + n\bar{\kappa}_{sz}(s, z) \quad (11b)$$

$$\gamma_{nz}(s, z, n) = \frac{\partial w}{\partial n} + \frac{\partial u}{\partial z} = \bar{\gamma}_{nz}(s, z) \quad (11c)$$

85 where

$$\bar{\epsilon}_z = \frac{\partial \bar{w}}{\partial z} = \epsilon_z^\circ + x\kappa_y + y\kappa_x + \omega\kappa_\omega \quad (12a)$$

$$\bar{\kappa}_z = \frac{\partial \bar{\psi}_z}{\partial z} = \kappa_y \sin \theta - \kappa_x \cos \theta - \kappa_\omega q \quad (12b)$$

$$\bar{\kappa}_{sz} = \frac{\partial \bar{\psi}_z}{\partial s} + \frac{\partial \bar{\psi}_s}{\partial z} = \kappa_{sz} \quad (12c)$$

86 The resulting strains can be obtained from Eqs.(??) and (??) as

$$\epsilon_z = \epsilon_z^\circ + (x + n \sin \theta)\kappa_y + (y - n \cos \theta)\kappa_x + (\omega - nq)\kappa_\omega \quad (13a)$$

$$\gamma_{sz} = \gamma_{xz}^\circ \cos \theta + \gamma_{yz}^\circ \sin \theta + \gamma_\omega^\circ r + n\kappa_{sz} \quad (13b)$$

$$\gamma_{nz} = \gamma_{xz}^\circ \sin \theta - \gamma_{yz}^\circ \cos \theta - \gamma_\omega^\circ q \quad (13c)$$

87 where $\epsilon_z^\circ, \kappa_x, \kappa_y, \kappa_\omega$ and κ_{sz} are axial strain, biaxial curvatures in the x and y direction, warping curvature with
88 respect to the shear center, and twisting curvature in the beam, respectively defined as

$$\epsilon_z^\circ = W' \quad (14a)$$

$$\kappa_x = \Psi'_x \quad (14b)$$

$$\kappa_y = \Psi'_y \quad (14c)$$

$$\kappa_\omega = \Psi'_\omega \quad (14d)$$

$$\kappa_{sz} = \Phi' - \Psi_\omega \quad (14e)$$

89 3. VARIATIONAL FORMULATION

90 The total potential energy of the system can be stated, in its buckled shape, as

$$\Pi = \mathcal{U} + \mathcal{V} \quad (15)$$

91 where \mathcal{U} is the strain energy

$$\mathcal{U} = \frac{1}{2} \int_v (\sigma_z \epsilon_z + \sigma_{sz} \gamma_{sz} + \sigma_{nz} \gamma_{nz}) dv \quad (16)$$

92 After substituting Eq.(??) into Eq.(??)

$$\begin{aligned} \mathcal{U} = & \frac{1}{2} \int_v \left\{ \sigma_z \left[\epsilon_z^\circ + (x + n \sin \theta) \kappa_y + (y - n \cos \theta) \kappa_x + (\omega - nq) \kappa_\omega \right] \right. \\ & \left. + \sigma_{sz} \left[\gamma_{xz}^\circ \cos \theta + \gamma_{yz}^\circ \sin \theta + \gamma_\omega^\circ r + n \kappa_{sz} \right] + \sigma_{nz} \left[\gamma_{xz}^\circ \sin \theta - \gamma_{yz}^\circ \cos \theta - \gamma_\omega^\circ q \right] \right\} dv \end{aligned} \quad (17)$$

93 The variation of strain energy, Eq.(??), can be stated as

$$\delta \mathcal{U} = \int_0^l (N_z \delta \epsilon_z + M_y \delta \kappa_y + M_x \delta \kappa_x + M_\omega \delta \kappa_\omega + V_x \delta \gamma_{xz}^\circ + V_y \delta \gamma_{yz}^\circ + T \delta \gamma_\omega^\circ + M_t \delta \kappa_{sz}) dz \quad (18)$$

94 where $N_z, M_x, M_y, M_\omega, V_x, V_y, T, M_t$ are axial force, bending moments in the x - and y -directions, warping mo-
95 ment (bimoment), and torsional moment with respect to the centroid, respectively, defined by integrating over the
96 cross-sectional area A as

$$N_z = \int_A \sigma_z ds dn \quad (19a)$$

$$M_y = \int_A \sigma_z (x + n \sin \theta) ds dn \quad (19b)$$

$$M_x = \int_A \sigma_z (y - n \cos \theta) ds dn \quad (19c)$$

$$M_\omega = \int_A \sigma_z (\omega - nq) ds dn \quad (19d)$$

$$V_x = \int_A (\sigma_{sz} \cos \theta + \sigma_{nz} \sin \theta) ds dn \quad (19e)$$

$$V_y = \int_A (\sigma_{sz} \sin \theta - \sigma_{nz} \cos \theta) ds dn \quad (19f)$$

$$T = \int_A (\sigma_{sz} r + \sigma_{nz} q) ds dn \quad (19g)$$

$$M_t = \int_A \sigma_{sz} n ds dn \quad (19h)$$

97 The potential of in-plane loads \mathcal{V} due to transverse deflection

$$\mathcal{V} = \frac{1}{2} \int_v \bar{\sigma}_z^0 [(u')^2 + (v')^2] dv \quad (20)$$

98 where $\bar{\sigma}_z^0$ is the averaged constant in-plane edge axial stress, defined by $\bar{\sigma}_z^0 = P_0/A$. The variation of the potential of
99 in-plane loads at the centroid is expressed by substituting the assumed displacement field into Eq.(??) as

$$\begin{aligned} \delta \mathcal{V} = & \int_v \frac{P_0}{A} \left[U' \delta U' + V' \delta V' + (q^2 + r^2 + 2rn + n^2) \Phi' \delta \Phi' + (\Phi' \delta U' + U' \delta \Phi') [n \cos \theta - (y - y_p)] \right. \\ & \left. + (\Phi' \delta V' + V' \delta \Phi') [n \cos \theta + (x - x_p)] \right] dv \end{aligned} \quad (21)$$

100 The kinetic energy of the system is given by

$$\mathcal{T} = \frac{1}{2} \int_v \rho (\dot{u}^2 + \dot{v}^2 + \dot{w}^2) dv \quad (22)$$

101 where ρ is a density.

102 The variation of the kinetic energy is expressed by substituting the assumed displacement field into Eq.(??) as

$$\begin{aligned} \delta\mathcal{T} = & \int_v \rho \left\{ \delta\dot{W} \left[\dot{W} + \dot{\Psi}_x(y - n \cos \theta) + \dot{\Psi}_y(x + n \sin \theta) + \dot{\Psi}_\omega(\omega - nq) \right] \right. \\ & + \delta\dot{U} \left[\dot{U} + \dot{\Phi} \left[n \cos \theta - (y - y_p) \right] \right] + \delta\dot{V} \left[m_0 \dot{V} + \dot{\Phi} \left[n \sin \theta + (x - x_p) \right] \right] \\ & + \delta\dot{\Phi} \dot{\Phi} \left[\dot{U} \left[n \cos \theta - (y - y_p) \right] + \dot{V} \left[n \sin \theta + (x - x_p) \right] + \dot{\Phi} (q^2 + r^2 + 2rn + n^2) \right] \\ & + \delta\dot{\Psi}_x \dot{\Psi}_x \left[\dot{W} (y - n \cos \theta) + \dot{\Psi}_x (y - n \cos \theta)^2 + \dot{\Psi}_y (x + n \sin \theta) (y - n \cos \theta) + \dot{\Psi}_\omega (y - n \cos \theta) (\omega - nq) \right] \\ & + \delta\dot{\Psi}_y \dot{\Psi}_y \left[\dot{W} (x + n \sin \theta) + \dot{\Psi}_x (x + n \sin \theta) (y - n \cos \theta) + \dot{\Psi}_y (x + n \sin \theta)^2 + \dot{\Psi}_\omega (x + n \sin \theta) (\omega - nq) \right] \\ & \left. + \delta\dot{\Psi}_\omega \dot{\Psi}_\omega \left[\dot{W} (\omega - nq) + \dot{\Psi}_x (y - n \cos \theta) (\omega - nq) + \dot{\Psi}_y (x + n \sin \theta) (\omega - nq) + \dot{\Psi}_\omega (\omega - nq)^2 \right] \right\} dv \quad (23) \end{aligned}$$

103 In order to derive the equations of motion, Hamilton's principle is used

$$\delta \int_{t_1}^{t_2} (\mathcal{T} - \Pi) dt = 0 \quad (24)$$

104 Substituting Eqs.(??), (??) and (??) into Eq.(??), the following weak statement is obtained

$$\begin{aligned} 0 = & \int_{t_1}^{t_2} \int_0^l \left\{ \delta\dot{W} \left[m_0 \dot{W} - m_c \dot{\Psi}_x + m_s \dot{\Psi}_y + (m_\omega - m_q) \dot{\Psi}_\omega \right] + \delta\dot{U} \left[m_0 \dot{U} + (m_c + y_p m_0) \dot{\Phi} \right] \right. \\ & + \delta\dot{V} \left[m_0 \dot{V} + (m_s - x_p m_0) \dot{\Phi} \right] + \delta\dot{\Phi} \left[(m_c + y_p m_0) \dot{U} + (m_s - x_p m_0) \dot{V} + (m_p + m_2 + 2m_r) \dot{\Phi} \right] \\ & + \delta\dot{\Psi}_x \left[-m_c \dot{W} + (m_{y2} - 2m_{yc} + m_{c2}) \dot{\Psi}_x + (m_{xycs} - m_{cs}) \dot{\Psi}_y + (m_{y\omega} - m_{y\omega qc} + m_{qc}) \dot{\Psi}_\omega \right] \\ & + \delta\dot{\Psi}_y \left[m_s \dot{W} + (m_{xycs} - m_{cs}) \dot{\Psi}_x + (m_{x2} + 2m_{xs} + m_{s2}) \dot{\Psi}_y + (m_{x\omega} + m_{x\omega qs} - m_{qs}) \dot{\Psi}_\omega \right] \\ & + \delta\dot{\Psi}_\omega \left[(m_\omega - m_q) \dot{W} + (m_{y\omega} - m_{y\omega qc} + m_{qc}) \dot{\Psi}_x + (m_{x\omega} + m_{x\omega qs} - m_{qs}) \dot{\Psi}_y + (m_{\omega 2} - 2m_{q\omega} + m_{q2}) \dot{\Psi}_\omega \right] \\ & - P_0 \left[\delta U' (U' + \Phi' y_p) + \delta V' (V' - \Phi' x_p) + \delta \Phi' \left(\Phi' \frac{I_p}{A} + U' y_p - V' x_p \right) \right] - N_z \delta W' \\ & \left. - M_y \delta \Psi'_y - M_x \delta \Psi'_x - M_\omega \delta \Psi'_\omega - V_x \delta (U' + \Psi_y) - V_y \delta (V' + \Psi_x) - T \delta (\Phi' - \Psi_\omega) - M_t \delta (\Phi' - \Psi_\omega) \right\} dz dt \quad (25) \end{aligned}$$

105 All the inertia coefficients in Eq.(??) are given in Ref.[?].

106 **4. CONSTITUTIVE EQUATIONS**

107 The constitutive equations of a k^{th} orthotropic lamina in the laminate co-ordinate system of section are given by

$$\begin{Bmatrix} \sigma_z \\ \sigma_{sz} \end{Bmatrix}^k = \begin{bmatrix} \bar{Q}_{11}^* & \bar{Q}_{16}^* \\ \bar{Q}_{16}^* & \bar{Q}_{66}^* \end{bmatrix}^k \begin{Bmatrix} \epsilon_z \\ \gamma_{sz} \end{Bmatrix} \quad (26)$$

108 where \bar{Q}_{ij}^* are transformed reduced stiffnesses. The transformed reduced stiffnesses can be calculated from the
 109 transformed stiffnesses based on the plane stress ($\sigma_s = 0$) and plane strain ($\epsilon_s = 0$) assumption. More detailed
 110 explanation can be found in Ref.[?].

111 The constitutive relation for out-of-plane stress and strain is given by

$$\sigma_{nz} = \bar{Q}_{55} \gamma_{nz} \quad (27)$$

112 The constitutive equations for bar forces and bar strains are obtained by using Eqs.(??), (??) and (??)

$$\begin{Bmatrix} N_z \\ M_y \\ M_x \\ M_\omega \\ M_t \\ V_x \\ V_y \\ T \end{Bmatrix} = \begin{bmatrix} E_{11} & E_{12} & E_{13} & E_{14} & E_{15} & E_{16} & E_{17} & E_{18} \\ & E_{22} & E_{23} & E_{24} & E_{25} & E_{26} & E_{27} & E_{28} \\ & & E_{33} & E_{34} & E_{35} & E_{36} & E_{37} & E_{38} \\ & & & E_{44} & E_{45} & E_{46} & E_{47} & E_{48} \\ & & & & E_{55} & E_{56} & E_{57} & E_{58} \\ & & & & & E_{66} & E_{67} & E_{68} \\ & & & & & & E_{77} & E_{78} \\ & & & & & & & E_{88} \end{bmatrix} \begin{Bmatrix} \epsilon_z^\circ \\ \kappa_y \\ \kappa_x \\ \kappa_\omega \\ \kappa_{sz} \\ \gamma_{xz}^\circ \\ \gamma_{yz}^\circ \\ \gamma_\omega^\circ \end{Bmatrix} \quad (28)$$

sym.

113 where E_{ij} are stiffnesses of thin-walled composite beams and given in Ref.[?].

114 **5. EQUATIONS OF MOTION**

115 The equations of motion of the present study can be obtained by integrating the derivatives of the varied quantities
 116 by parts and collecting the coefficients of $\delta W, \delta U, \delta V, \delta \Phi, \delta \Psi_y, \delta \Psi_x$ and $\delta \Psi_\omega$

$$N'_z = m_0 \ddot{W} - m_c \ddot{\Psi}_x + m_s \ddot{\Psi}_y + (m_\omega - m_q) \ddot{\Psi}_\omega \quad (29a)$$

$$V'_x + P_0(U'' + \Phi'' y_p) = m_0 \ddot{U} + (m_c + y_p m_0) \ddot{\Phi} \quad (29b)$$

$$V'_y + P_0(V'' - \Phi'' x_p) = m_0 \ddot{V} + (m_s - x_p m_0) \ddot{\Phi} \quad (29c)$$

$$\begin{aligned} M'_t + T' + P_0\left(\Phi'' \frac{I_p}{A} + U'' y_p - V'' x_p\right) &= (m_c - m_y + y_p m_0) \ddot{U} + (m_s - x_p m_0) \ddot{V} \\ &+ (m_p + m_2 + 2m_r) \ddot{\Phi} \end{aligned} \quad (29d)$$

$$\begin{aligned} M'_y - V_x &= m_s \ddot{W} + (m_{xycs} - m_{cs}) \ddot{\Psi}_x + (m_{x2} + 2m_{xs} + m_{s2}) \ddot{\Psi}_y \\ &+ (m_{x\omega} + m_{x\omega qs} - m_{qs}) \ddot{\Psi}_\omega \end{aligned} \quad (29e)$$

$$\begin{aligned} M'_x - V_y &= -m_c \ddot{W} + (m_{y2} - 2m_{yc} + m_{c2}) \ddot{\Psi}_x + (m_{xycs} - m_{cs}) \ddot{\Psi}_y \\ &+ (m_{y\omega} - m_{y\omega qc} + m_{qc}) \ddot{\Psi}_\omega \end{aligned} \quad (29f)$$

$$\begin{aligned} M'_\omega + M_t - T &= (m_\omega - m_q) \ddot{W} + (m_{y\omega} - m_{y\omega qc} + m_{qc}) \ddot{\Psi}_x \\ &+ (m_{x\omega} + m_{x\omega qs} - m_{qs}) \ddot{\Psi}_y \\ &+ (m_{\omega 2} - 2m_{q\omega} + m_{q2}) \ddot{\Psi}_\omega \end{aligned} \quad (29g)$$

117 The natural boundary conditions are of the form

$$\delta W : \quad W = \bar{W}_0 \quad \text{or} \quad N_z = P_0 \quad (30a)$$

$$\delta U : \quad U = \bar{U}_0 \quad \text{or} \quad V_x = \bar{V}_{x_0} \quad (30b)$$

$$\delta V : \quad V = \bar{V}_0 \quad \text{or} \quad V_y = \bar{V}_{y_0} \quad (30c)$$

$$\delta \Phi : \quad \Phi = \bar{\Phi}_0 \quad \text{or} \quad T + M_t = \bar{T}_0 + \bar{M}_{t_0} \quad (30d)$$

$$\delta \Psi_y : \quad \Psi_y = \bar{\Psi}_{y_0} \quad \text{or} \quad M_y = \bar{M}_{y_0} \quad (30e)$$

$$\delta \Psi_x : \quad \Psi_x = \bar{\Psi}_{x_0} \quad \text{or} \quad M_x = \bar{M}_{x_0} \quad (30f)$$

$$\delta \Psi_\omega : \quad \Psi_\omega = \bar{\Psi}_{\omega_0} \quad \text{or} \quad M_\omega = \bar{M}_{\omega_0} \quad (30g)$$

118 The 7th denotes the warping restraint boundary condition. When the warping of the cross section is restrained,
 119 $\Psi_\omega = 0$ and when the warping is not restrained, $M_\omega = 0$.

Eq.(??) is most general form for free vibration of thin-walled composite Timoshenko beams under a constant axial force. For general anisotropic materials, the dependent variables, U , V , W , Φ , Ψ_x , Ψ_y and Ψ_ω are fully-coupled implying that the beam undergoes a coupled behavior involving bending, extension, twisting, transverse shearing, and warping. The resulting coupling is referred to as sixfold coupled vibrations. If all the coupling effects are neglected and cross section is symmetrical with respect to both x - and the y -axes, Eq.(??) can be simplified to the uncoupled differential equations as

$$(EA)_{com}W'' = \rho A\ddot{W} \quad (31a)$$

$$(GA_y)_{com}(U'' + \Psi'_y) + P_0U'' = \rho A\ddot{U} \quad (31b)$$

$$(GA_x)_{com}(V'' + \Psi'_x) + P_0V'' = \rho A\ddot{V} \quad (31c)$$

$$\left[(GJ_1)_{com} + P_0\frac{I_p}{A}\right]\Phi'' - (GJ_2)_{com}\Psi'_\omega = \rho I_p\ddot{\Phi} \quad (31d)$$

$$(EI_y)_{com}\Psi''_y - (GA_y)_{com}(U' + \Psi_y) = \rho I_y\ddot{\Psi}_y \quad (31e)$$

$$(EI_x)_{com}\Psi''_x - (GA_x)_{com}(V' + \Psi_x) = \rho I_x\ddot{\Psi}_x \quad (31f)$$

$$(EI_\omega)_{com}\Psi''_\omega + (GJ_2)_{com}\Phi' - (GJ_1)_{com}\Psi_\omega = \rho I_\omega\ddot{\Psi}_\omega \quad (31g)$$

It is well known that the three distinct vibration mode, flexural vibration in the x - and y -direction and torsional vibration are identified in this case. From above equations, $(EA)_{com}$ represents axial rigidity, $(GA_x)_{com}$, $(GA_y)_{com}$ represent shear rigidities with respect to x and y axis, $(EI_x)_{com}$ and $(EI_y)_{com}$ represent flexural rigidities with respect to x - and y -axis, $(EI_\omega)_{com}$ represents warping rigidity, and $(GJ_1)_{com}$, $(GJ_2)_{com}$ represent torsional rigidities of thin-walled composite beams, respectively, written as

$$(EA)_{com} = E_{11} \quad (32a)$$

$$(EI_y)_{com} = E_{22} \quad (32b)$$

$$(EI_x)_{com} = E_{33} \quad (32c)$$

$$(EI_\omega)_{com} = E_{44} \quad (32d)$$

$$(GA_y)_{com} = E_{66} \quad (32e)$$

$$(GA_x)_{com} = E_{77} \quad (32f)$$

$$(GJ_1)_{com} = E_{55} + E_{88} \quad (32g)$$

$$(GJ_2)_{com} = E_{55} - E_{88} \quad (32h)$$

131 6. FINITE ELEMENT FORMULATION

132 The present theory for thin-walled composite Timoshenko beams described in the previous section is implemented
 133 via a one-dimensional displacement-based finite element method. The same interpolation function is used for all the
 134 translational and rotational displacements. Reduced integration of shear terms, that is, stiffness coefficients involving
 135 laminate stiffnesses ($E_{i,j}$, $i = 6..8, j = 6..8$) is used to avoid shear locking. The generalized displacements are expressed
 136 over each element as a combination of the one-dimensional Lagrange interpolation function $\widehat{\phi}_j$ associated with node
 137 j and the nodal values

$$W = \sum_{j=1}^n w_j \widehat{\phi}_j \quad (33a)$$

$$U = \sum_{j=1}^n u_j \widehat{\phi}_j \quad (33b)$$

$$V = \sum_{j=1}^n v_j \widehat{\phi}_j \quad (33c)$$

$$\Phi = \sum_{j=1}^n \phi_j \widehat{\phi}_j \quad (33d)$$

$$\Psi_y = \sum_{j=1}^n \psi_{yj} \widehat{\phi}_j \quad (33e)$$

$$\Psi_x = \sum_{j=1}^n \psi_{xj} \widehat{\phi}_j \quad (33f)$$

$$\Psi_\omega = \sum_{j=1}^n \psi_{\omega j} \widehat{\phi}_j \quad (33g)$$

138 where n is the number of nodes in an element and Lagrange interpolation function $\widehat{\phi}_j$ for linear, quadratic and cubic
 139 elements are available in the literature.

140 Substituting these expressions into the weak statement in Eq.(??), the finite element model of a typical element
 141 can be expressed as

$$([K] - P_0[G] - \omega^2[M])\{\Delta\} = \{0\} \quad (34)$$

142 where $[K]$, $[G]$ and $[M]$ are the element stiffness matrix, the element geometric stiffness matrix and the element mass
 143 matrix, respectively. The explicit forms of them are given in Refs.[?/?].

144 In Eq.(??), $\{\Delta\}$ is the eigenvector of nodal displacements corresponding to an eigenvalue

$$\{\Delta\} = \{W \ U \ V \ \Phi \ \Psi_y \ \Psi_x \ \Psi_\omega\}^T \quad (35)$$

145 7. NUMERICAL EXAMPLES

146 For verification purpose, the buckling behavior and free vibration of a cantilever symmetrically laminated mono-
 147 symmetric I-beam with length $l = 1\text{m}$ under axial load at the centroid is considered. Following dimensions for
 148 the I-beam are used: the height, top and bottom flange widths are 50mm, 30mm and 50mm, respectively. The
 149 flanges and web are made of sixteen layers with each layer 0.13mm in thickness. All computations are carried out
 150 for the glass-epoxy materials with the following material properties: $E_1 = 53.78\text{GPa}$, $E_2 = 17.93\text{GPa}$, $G_{12} =$
 151 $G_{13} = 8.96\text{GPa}$, $G_{23} = 3.45\text{GPa}$, $\nu_{12} = 0.25$, $\rho = 1968.9\text{kg/m}^3$. **In Table ??, the critical buckling loads are**
 152 **compared with numerical results of Kim and Shin [?], which is based on dynamic stiffness formulation**
 153 **and ABAQUS solution by using nine-noded shell element (S9R5). It is clear that the numerical**
 154 **solution using ABAQUS always underestimates the analytical solution except for $[60/-60]_{4s}$ lay-up.**
 155 **However, the buckling load of this case is overestimated approximate by 3%, which is an acceptable**
 156 **error.** Next, the flexural-torsional coupled vibration analysis of axially loaded cantilever beam is evaluated. The
 157 applied magnitude of axial force is given in Ref. [?], which corresponds to one half of buckling load of beam. The
 158 lowest four coupled natural frequencies with and without the axial force are presented in Table ?. It reveals that
 159 the tension force has a stiffening effect while the compressive force has a softening effect on the natural frequencies of
 160 the beam. It can be seen from Tables ?? and ?? that the present results are in a good agreement with those by Kim
 161 and Shin [?].

162 In order to investigate the effects of axial force, fiber orientation and shear deformation on the natural frequencies
 163 and corresponding vibration mode shapes as well as load-frequency interaction curves, thin-walled composite I-beams
 164 with length $l = 3\text{m}$ and various boundary conditions under axial load at the centroid are considered. The geometry
 165 and stacking sequences of I-section are shown in Fig.??, and the following engineering constants are used

$$E_1/E_2 = 25, G_{12}/E_2 = 0.6, G_{13} = G_{12} = G_{23}, \nu_{12} = 0.25 \quad (36)$$

166 For convenience, the following nondimensional buckling load and natural frequency are used

$$\bar{P} = \frac{P_0 l^2}{b_3^3 t E_2} \quad (37)$$

$$\bar{\omega} = \frac{\omega l^2}{b_3} \sqrt{\frac{\rho}{E_2}} \quad (38)$$

167 As a first example, a simply supported composite I-beam is considered. Stacking sequences of the flanges and web
 168 are angle-ply laminates $[\theta/-\theta]$, (Fig. ??a). For this lay-up, all the coupling stiffnesses are zero, but E_{35} and E_{38}

do not vanish due to unsymmetric stacking sequence of the flanges and web. In Table ??, effects of axial force and flexural-torsional coupling on the lowest four natural frequencies are inspected. This demonstrates again the well-known fact that a tensile force stiffens the beam and a compressive force softens the beam. The uncoupled solution, which neglects the coupling effects, is also given. The critical buckling loads agree completely with those of previous paper [?], as expected. Due to coupling stiffnesses, the uncoupled solution might not be accurate. However, as fiber angle increases, the coupling effects coming from the material anisotropy become negligible. It can be seen in Table ?? that for all cases of fiber angles, the lowest four natural frequencies by the coupled solution always correspond to the first flexural mode in x -direction, the the first torsional mode, the first flexural mode in y -direction and the second flexural mode in x -direction by the uncoupled solution, respectively. It is indicated that the uncoupled solution is sufficiently accurate for this lay-up. It can be explained partly by the typical normal mode shapes with fiber angle $\theta = 30^\circ$ for the case of axial compressive force ($\bar{P} = 0.5\bar{P}_{cr}$) in Fig.?.?. The mode shapes for other cases of axial force ($\bar{P} = 0$ and $\bar{P} = -0.5\bar{P}_{cr}$) are similar to the corresponding ones for the case of axial force ($\bar{P} = 0.5\bar{P}_{cr}$) and are not plotted, although there is a little difference between them. Three dimensional fiber-axial-frequency interaction diagram with respect to the fiber angle change is illustrated in Fig. ?.?. Four groups of curves corresponding to $\omega_1, \omega_2, \omega_3$ and ω_4 are observed. It is interesting to see that two larger groups, $(\omega_3 - P_3)$ and $(\omega_4 - P_4)$, always intersect each other for all fiber angles. To investigate the effects of shear deformation on the load-frequency interaction curves, the stacking sequence at fiber angles $\theta = 0^\circ, 30^\circ$ and 60° is considered. The lowest four load-frequency interaction curves at these fiber angles are shown in Figs.??-??. These curves obtained from previous research [?] based on the classical beam theory are also displayed. It is obvious that the natural frequencies decrease with the increase of axial force, and the decrease becomes more quickly when the axial force is close to buckling loads. Shear effects are more pronounced with unidirectional fiber direction (Fig.??) and decrease as fiber angle increases (Figs.?? and ??). This trend can be explained that flexural stiffnesses decrease significantly with increasing fiber angle, and thus, the relative shear effects become smaller for the higher fiber angles. Figs.??-?? also explain the duality between the flexural-torsional buckling loads and the natural frequencies.

To investigate the coupling and shear effects further, a clamped composite I-beam is performed. The bottom flange is considered as $[\theta_2]$, while the top flange and web are $[0/45]$, respectively (Fig.??b). For this lay-up, the coupling stiffnesses $E_{16}, E_{17}, E_{18}, E_{36}, E_{37}$ and E_{68} become no more negligibly small. Major effects of axial force and shear deformation on the natural frequencies are again seen in Table ?.?. It is indicated that the solutions excluding shear effects remarkably underestimate the natural frequencies for all fiber angles. This implies that discarding shear effects

198 leads to an overprediction of the natural frequencies. The interaction diagram between the flexural-torsional buckling
 199 loads and natural frequencies by the coupled and uncoupled solution with the fiber angle $\theta = 0^\circ$ and 60° are displayed
 200 in Figs.?? and ??. Characteristic of load-frequency interaction curves is that the value of the axial force for which
 201 the natural frequencies vanish constitute the buckling loads. Thus, for $\theta = 60^\circ$, the first and second flexural-torsional
 202 bucklings occur at $\bar{P} = 2.861$ and 5.695 . As a result, the lowest two branches vanish when \bar{P} is slightly over $\bar{P} = 5.695$.
 203 As the axial force increases, two interaction curves $(w_3 - P_3)$ and $(w_4 - P_4)$ intersect at $\bar{P} = 9.413$, thus, after this
 204 value, the phenomenon of mode shifting for mode 3 and 4 can be observed. Finally, the third and fourth branch will
 205 also disappear when \bar{P} is slightly over 10.790 and 15.641 , respectively. The typical normal mode shapes corresponding
 206 to the lowest four natural frequencies with fiber angle $\theta = 30^\circ$ for the case of axial compressive force ($\bar{P} = 0.5\bar{P}_{cr}$)
 207 are illustrated in Fig.?.?. Relative measures of flexural displacements, torsional and shearing rotation show that when
 208 the beam is vibrating at the natural frequency belonging to the first and second mode exhibit fourfold coupled modes
 209 (flexural vibration in the x -direction, torsional and corresponding shearing vibration), whereas, third and fourth
 210 mode display sixfold coupled modes (flexural mode in the x -, y -direction, torsional mode and corresponding shearing
 211 vibration). This fact explains as the fiber angle changes, for lower span-to-height ratio, the uncoupled solution disagree
 212 with coupled solution as anisotropy of the beam gets higher. That is, the uncoupled solution is no longer valid for
 213 unsymmetrically laminated beams, and sixfold flexural-torsional-shearing coupled vibrations should be considered
 214 even for a doubly symmetric cross-section.

215 Finally, the effects of modulus ratio (E_1/E_2) on the first three natural frequencies of a cantilever composite I-beam
 216 under axial compressive force and tensile force with value $(0.5\bar{P}_{cr})$ are investigated. The stacking sequence of the
 217 flanges and web are $[0/90]_s$, (Fig.??c). For this lay-up, all the coupling stiffnesses vanish and thus, the three distinct
 218 vibration mode, flexural vibration in the x - and y -direction and torsional vibration are identified. It is observed
 219 from Fig.?? that the natural frequencies ω_{x_1} , ω_{θ_1} and ω_{y_1} increase with increasing orthotropy (E_1/E_2) for two cases
 220 considered.

221 8. CONCLUDING REMARKS

222 A analytical model based on shear-deformable beam theory is developed to study free vibration of axially loaded
 223 thin-walled composite Timoshenko beams with arbitrary lay-ups. This model is capable of predicting accurately the
 224 natural frequencies, load-frequency interaction curves as well as corresponding vibration mode shapes for various
 225 configuration. All of the possible vibration mode shapes including the flexural mode in the x - and y -direction, the

226 torsional mode, and fully coupled flexural-torsional-shearing mode are included in the analysis. The shear effects
227 become significant for lower span-to-height ratio. The present model is found to be appropriate and efficient in
228 analyzing free vibration problem of axially loaded thin-walled composite Timoshenko beams.

229 Acknowledgments

230 This research was supported by Basic Research Laboratory Program of the National Research Foundation of Korea
231 (NRF) funded by the Ministry of Education, Science and Technology through NRF2010-0019373, and by Korea
232 Ministry of Knowledge Economy under the national HRD support program for convergence information technology
233 supervised by National IT Industry Promotion Agency through NIPA-2010-C6150-1001-0013. The authors also would
234 like to thank the anonymous reviewers for their suggestions in improving the standard of the manuscript.

235 References

- 236 Vlasov, V. Z. (1961) *Thin Walled Elastic Beams*. Israel Program for Scientific Transactions, Jerusalem.
- 237 Gjelsvik, A. (1981) *The theory of thin walled bars*. Wiley, New York.
- 238 Bleich, F., Ramsey, L., and Bleich, H. (1952) *Buckling strength of metal structures*. McGraw-Hill, New York.
- 239 Timoshenko, S. and Gere, J. M. (1961) *Theory of elastic stability*. McGraw-Hill, New York.
- 240 Timoshenko, S., Young, D. H., and Weaver, W. J. R. (1974) *Vibration problems in engineering*. John Wiley & Sons, New York.
- 241 Bank, L. C. and Kao, C. (1990) Dynamic Response of Thin-Walled Composite Material Timoshenko Beams. *J Energ Resour*,
242 **112**, 149–154.
- 243 Cortinez, V. H. and Piovan, M. T. (2002) Vibration and buckling of composite thin-walled beams with shear deformability. *J*
244 *Sound Vib*, **258**, 701 – 723.
- 245 Machado, S. P. and Cortinez, V. H. (2007) Free vibration of thin-walled composite beams with static initial stresses and
246 deformations. *Eng Struct*, **29**, 372 – 382.
- 247 Banerjee, J. R. and Williams, F. W. (1996) Exact dynamic stiffness matrix for composite Timoshenko beams with applications.
248 *J Sound Vib*, **194**, 573 – 585.
- 249 Banerjee, J. R. (1998) Free vibration of axially loaded composite Timoshenko beams using the dynamic stiffness matrix method.
250 *Comput Struct*, **69**, 197 – 208.
- 251 Banerjee, J. R., Su, H., and Jayatunga, C. (2008) A dynamic stiffness element for free vibration analysis of composite beams
252 and its application to aircraft wings. *Comput Struct*, **86**, 573 – 579.

- 253 Li, J., Shen, R., Hua, H., and Xianding, J. (2004) Bending-torsional coupled dynamic response of axially loaded composite
254 Timoshenko thin-walled beam with closed cross-section. *Compos Struct*, **64**, 23 – 35.
- 255 Li, J., Wu, G., Shen, R., and Hua, H. (2005) Stochastic bending-torsion coupled response of axially loaded slender composite-
256 thin-walled beams with closed cross-sections. *Int J Mech Sci*, **47**, 134 – 155.
- 257 Kaya, M. and Ozgumus, O. O. (2007) Flexural-torsional-coupled vibration analysis of axially loaded closed-section composite
258 Timoshenko beam by using DTM. *J Sound Vib*, **306**, 495 – 506.
- 259 Kim, N. I., Shin, D. K., and Park, Y. S. (2008) Dynamic stiffness matrix of thin-walled composite I-beam with symmetric and
260 arbitrary laminations. *J Sound Vib*, **318**, 364 – 388.
- 261 Kim, N. I. and Shin, D. K. (2009) Dynamic stiffness matrix for flexural-torsional, lateral buckling and free vibration analyses
262 of mono-symmetric thin-walled composite beams. *Int J Struct Stab Dy*, **9**, 411–436.
- 263 Lee, J. (2005) Flexural analysis of thin-walled composite beams using shear-deformable beam theory. *Compos Struct*, **70**, 212
264 – 222.
- 265 Vo, T. P. and Lee, J. (2009) On sixfold coupled buckling of thin-walled composite beams. *Compos Struct*, **90**, 295 – 303.
- 266 Vo, T. P., Lee, J., and Ahn, N. (2009) On sixfold coupled vibrations of thin-walled composite box beams. *Compos Struct*, **89**,
267 524 – 535.
- 268 Jones, R. M. (1999) *Mechanics of Composite Materials*. Taylor & Francis.
- 269 Vo, T. P. and Lee, J. (2010) On triply coupled vibrations of axially loaded thin-walled composite beams. *Comput Struct*, **88**,
270 144–153.

271 **CAPTIONS OF TABLES**

272 Table ??: Critical bucking loads (N) of a cantilever mono-symmetric composite I-beam with symmetric angle-ply
273 laminates $[\pm\theta]_{4s}$ in the flanges and web.

274 Table ??: Effect of axial force on the first four natural frequencies (Hz) of a cantilever mono-symmetric composite
275 I-beam with symmetric angle-ply laminates $[\pm\theta]_{4s}$ in the flanges and web under constant axial forces at the centroid
276 ((): natural frequency with an axial compressive force, []: natural frequency with an axial tensile force).

277 Table ??: Effect of axial force on the first four natural frequencies with respect to the fiber angle change in the
278 flanges and web of a simply supported composite beam.

279 Table ??: Effect of axial force on the first four natural frequencies with respect to the fiber angle change in the
280 bottom flange of a clamped composite beam.

281 **CAPTIONS OF FIGURES**

282 Figure ??: Definition of coordinates and generalized displacements in thin-walled open sections.

283 Figure ??: Geometry and stacking sequences of thin-walled composite I-beam.

284 Figure ??: The first four normal mode shapes of the flexural, torsional and corresponding shearing components
 285 with the fiber angle 30° in the flanges and web of a simply supported composite beam under an axial compressive
 286 force ($\bar{P} = 0.5\bar{P}_{cr}$).

287 Figure ??: Three dimensional interaction diagram between between axial force and the first four natural frequencies
 288 with respect to the fiber angle change in the flanges and web of a simply supported composite beam.

289 Figure ??: Effect of axial force on the first four natural frequencies with the fiber angle 0° in the flanges and web
 290 of a simply supported composite beam.

291 Figure ??: Effect of axial force on the first four natural frequencies with the fiber angle 30° in the flanges and web
 292 of a simply supported composite beam.

293 Figure ??: Effect of axial force on the first four natural frequencies with the fiber angle 60° in the flanges and web
 294 of a simply supported composite beam.

295 Figure ??: Effect of axial force on the first four natural frequencies with the fiber angle 0° in the bottom flange of
 296 a clamped composite beam.

297 Figure ??: Effect of axial force on the first four natural frequencies with the fiber angle 60° in the bottom flange of
 298 a clamped composite beam.

299 Figure ??: The first four normal mode shapes of the flexural, torsional and corresponding shearing components with
 300 the fiber angle 30° in the bottom flange of a clamped composite beam under an axial compressive force ($\bar{P} = 0.5\bar{P}_{cr}$).

301 Figure ??: Variation of the first three natural frequencies with respect to modulus ratio change of a cantilever
 302 composite beam under an axial compressive force ($\bar{P} = 0.5\bar{P}_{cr}$) and an axial tensile force ($\bar{P} = -0.5\bar{P}_{cr}$).

TABLE 1 Critical bucking loads (N) of a cantilever mono-symmetric composite I-beam with symmetric angle-ply laminates $[\pm\theta]_{4s}$ in the flanges and web.

Lay-ups	Kim and Shin [?]		Present
	ABAQUS	Analytical	
$[0]_{16}$	2969.7	2998.1	2993.2
$[15/-15]_{4s}$	2790.9	2813.8	2803.6
$[30/-30]_{4s}$	2190.6	2201.1	2184.7
$[45/-45]_{4s}$	1558.9	1562.4	1546.0
$[60/-60]_{4s}$	1239.4	1241.5	1277.8
$[75/-75]_{4s}$	1132.2	1134.5	1126.7

TABLE 2 Effect of axial force on the first four natural frequencies (Hz) of a cantilever mono-symmetric composite I-beam with symmetric angle-ply laminates $[\pm\theta]_{4s}$ in the flanges and web under constant axial forces at the centroid ((): natural frequency with an axial compressive force, []: natural frequency with an axial tensile force).

Mode	Stacking sequences and values of axial force											
	[0] ₁₆		[15/ - 15] _{4s}		[30/ - 30] _{4s}		[45/ - 45] _{4s}		[60/ - 60] _{4s}		[75/ - 75] _{4s}	
	$P_0=1499.05$ N		$P_0=1406.90$ N		$P_0=1100.55$ N		$P_0=781.20$ N		$P_0=620.75$ N		$P_0=567.25$ N	
	Ref. [?]	Present	Ref. [?]	Present	Ref. [?]	Present	Ref. [?]	Present	Ref. [?]	Present	Ref. [?]	Present
1	(19.087)	(19.049)	(18.505)	(18.433)	(16.401)	(16.273)	(13.841)	(13.686)	(12.342)	(12.196)	(11.791)	(11.705)
	26.295	26.258	25.508	25.449	22.641	22.538	19.130	19.003	17.063	16.942	16.294	16.223
	[31.498]	[31.457]	[30.568]	[30.509]	[27.162]	[27.062]	[22.970]	[22.844]	[20.492]	[20.371]	[19.561]	[19.491]
2	(43.267)	(43.140)	(44.524)	(44.262)	(46.335)	(45.047)	(40.135)	(40.011)	(35.692)	(35.585)	(34.273)	(34.160)
	46.472	46.335	47.346	47.091	48.325	47.100	42.243	42.115	37.575	37.465	36.066	35.949
	[49.414]	[49.268]	[49.969]	[49.716]	[50.213]	[49.042]	[44.224]	[44.091]	[39.345]	[39.231]	[37.751]	[37.630]
3	(59.242)	(58.864)	(56.205)	(55.895)	(48.304)	(48.110)	(45.879)	(42.703)	(42.648)	(39.083)	(37.990)	(36.413)
	61.988	61.600	58.920	58.600	50.772	50.572	47.267	44.199	43.831	40.377	39.210	37.687
	[64.586]	[64.185]	[61.484]	[61.152]	[53.096]	[52.889]	[48.593]	[45.626]	[44.963]	[41.612]	[40.374]	[38.902]
4	(129.73)	(129.088)	(127.28)	(126.499)	(118.02)	(116.392)	(104.11)	(101.485)	(93.778)	(91.117)	(88.027)	(86.615)
	138.17	137.528	135.30	134.535	124.68	123.143	109.44	106.946	98.472	95.946	92.605	91.261
	[146.02]	[145.376]	[142.77]	[142.020]	[130.94]	[129.469]	[114.47]	[112.091]	[102.92]	[100.501]	[96.927]	[95.640]

TABLE 3 Effect of axial force on the first four natural frequencies with respect to the fiber angle change in the flanges and web of a simply supported composite beam.

Fiber angle	Buckling loads (\bar{P}_{cr})	Axial force \bar{P}	Uncoupled solution				Coupled solution			
			w_{x_1}	w_{θ_1}	w_{y_1}	w_{x_2}	w_1	w_2	w_3	w_4
0	11.214		4.866	5.885	15.023	22.687	4.866	5.885	15.023	22.687
30	3.290	$0.5\bar{P}_{cr}$	2.635	3.379	10.000	13.691	2.635	3.333	9.994	13.690
60	0.602	(compression)	1.127	1.520	4.397	5.914	1.127	1.515	4.396	5.914
90	0.486		1.012	1.345	3.951	5.311	1.012	1.345	3.951	5.311
0	11.214		6.881	7.635	15.789	24.680	6.881	7.635	15.788	24.680
30	3.290	0	3.727	4.285	10.337	14.665	3.727	4.249	10.332	14.664
60	0.602	(no axial force)	1.594	1.892	4.537	6.326	1.594	1.888	4.536	6.326
90	0.486		1.432	1.683	4.077	5.682	1.432	1.683	4.077	5.682
0	11.214		8.427	9.053	16.518	26.524	8.427	9.053	16.518	26.524
30	3.290	$-0.5\bar{P}_{cr}$	4.565	5.030	10.664	15.578	4.564	4.999	10.660	15.577
60	0.602	(tension)	1.952	2.202	4.673	6.714	1.952	2.199	4.672	6.713
90	0.486		1.753	1.964	4.199	6.030	1.753	1.964	4.199	6.030

TABLE 4 Effect of axial force on the first four natural frequencies with respect to the fiber angle change in the bottom flange of a clamped composite beam.

Fiber angle	Buckling loads (\bar{P}_{cr})	Axial force \bar{P}	No shear ([?])				Present			
			w_1	w_2	w_3	w_4	w_1	w_2	w_3	w_4
0	29.582		10.477	12.438	33.759	38.188	8.370	10.509	21.035	24.770
30	15.918	$0.5\bar{P}_{cr}$	6.965	9.433	23.078	28.958	6.183	9.444	17.690	20.444
60	2.861	(compression)	2.858	9.481	9.524	19.879	2.725	8.965	11.192	18.145
90	2.290		2.558	8.517	9.491	17.773	2.449	8.050	11.293	16.480
0	29.582		13.734	15.277	37.850	39.199	11.564	14.252	22.527	29.090
30	15.918	0	9.540	11.458	26.275	30.448	8.646	11.836	19.009	23.219
60	2.861	(no axial force)	3.975	9.871	10.911	21.351	3.805	10.305	11.753	18.325
90	2.290		3.557	9.758	9.805	19.091	3.422	9.258	11.748	17.767
0	-29.582		16.306	17.628	40.180	41.516	13.957	17.094	23.913	32.762
30	-15.918	$-0.5\bar{P}_{cr}$	11.512	13.151	29.100	31.129	10.495	13.767	20.038	25.815
60	-2.861	(tension)	4.823	10.246	12.131	22.725	4.612	11.472	12.287	18.502
90	-2.290		4.315	10.107	10.850	20.321	4.149	10.310	12.185	18.364

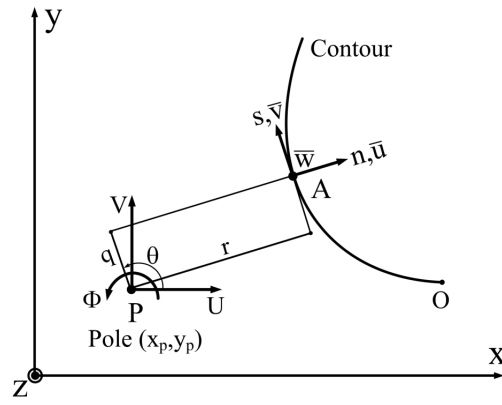


FIG. 1 Definition of coordinates in thin-walled open sections.

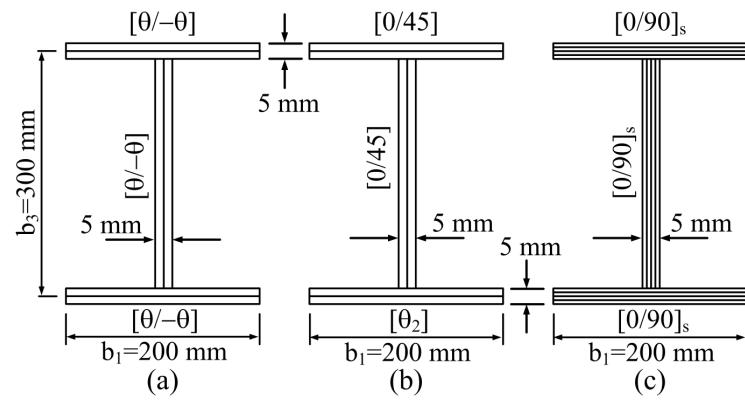


FIG. 2 Geometry and stacking sequences of thin-walled composite I-beam.

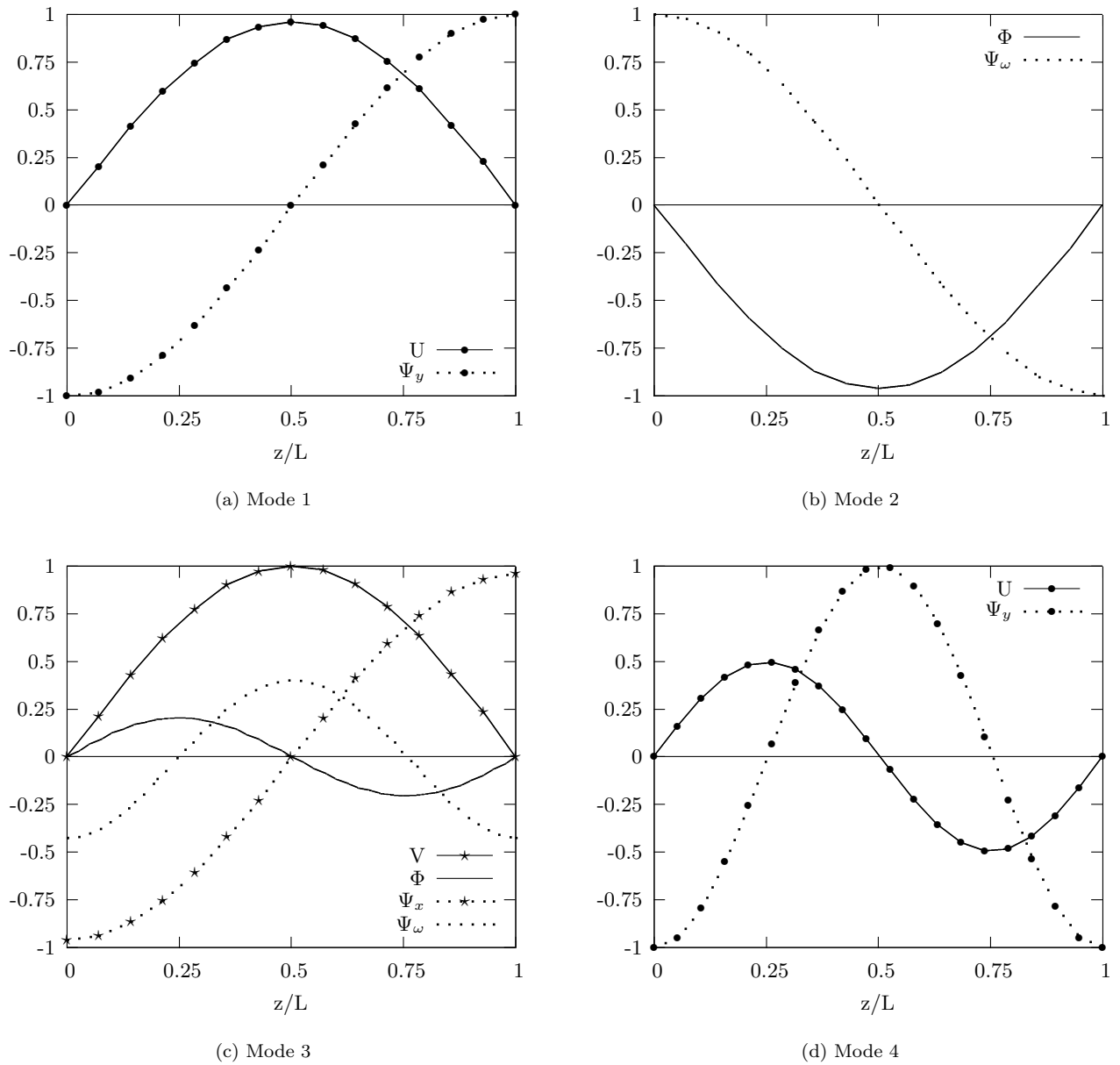


FIG. 3 The first four normal mode shapes of the flexural, torsional and corresponding shearing components with the fiber angle 30° in the flanges and web of a simply supported composite beam under an axial compressive force ($\bar{P} = 0.5\bar{P}_{cr}$).

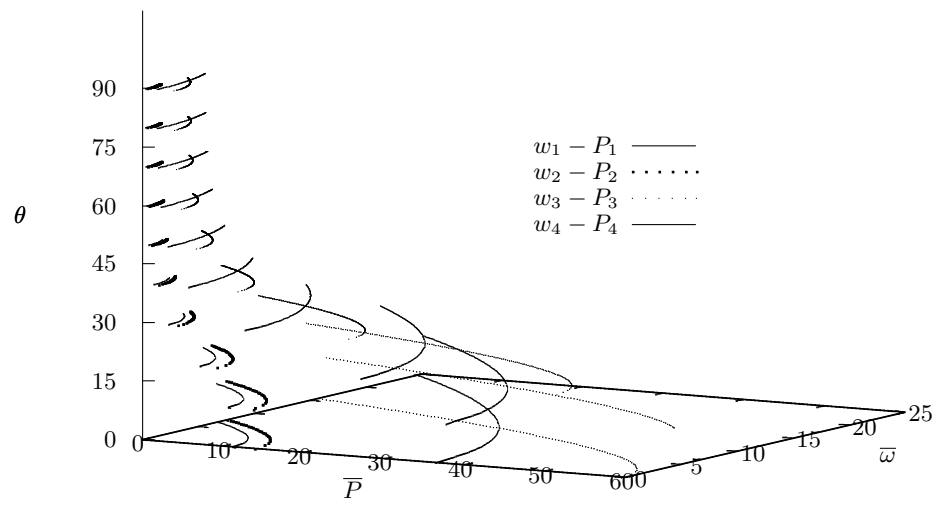


FIG. 4 Three dimensional interaction diagram between axial force and the first four natural frequencies with respect to the fiber angle change in the flanges and web of a simply supported composite beam.

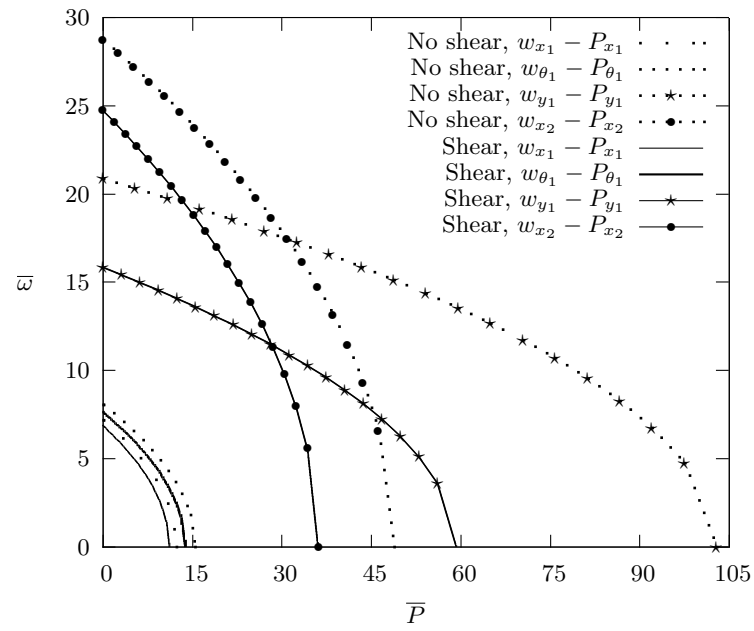


FIG. 5 Effect of axial force on the first four natural frequencies with the fiber angle 0° in the flanges and web of a simply supported composite beam.

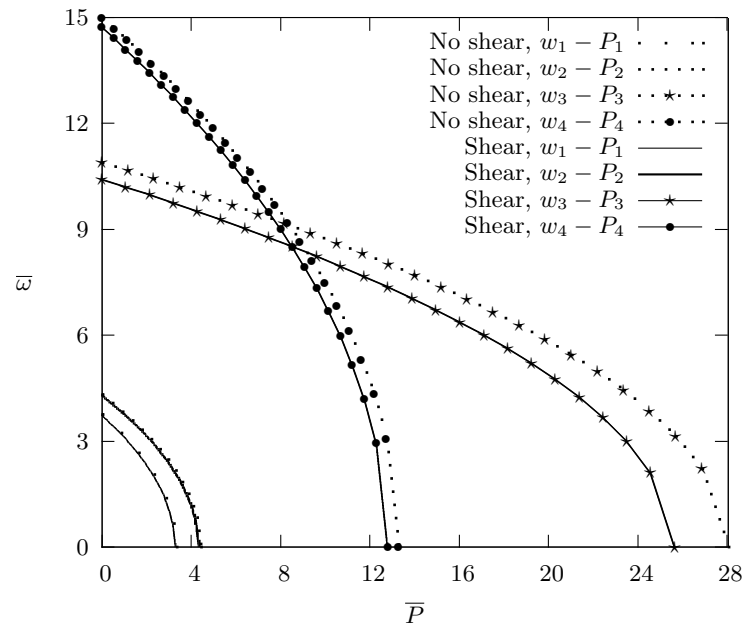


FIG. 6 Effect of axial force on the first four natural frequencies with the fiber angle 30° in the flanges and web of a simply supported composite beam.

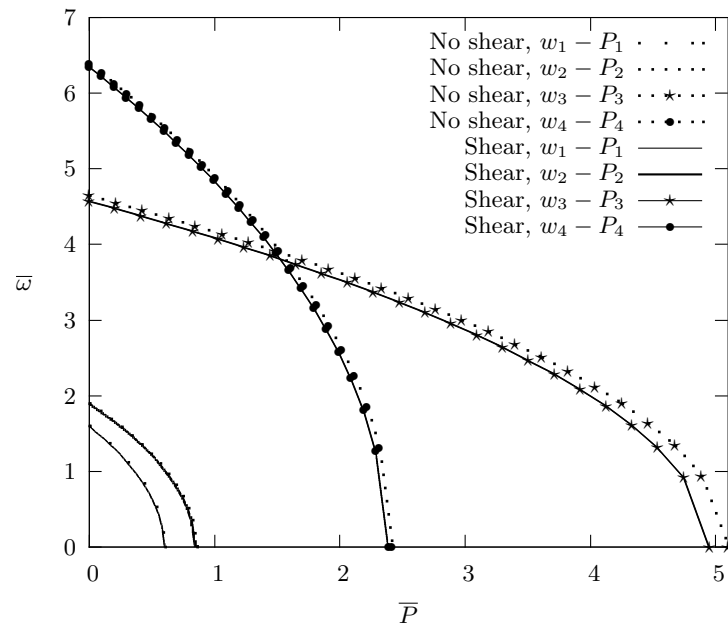


FIG. 7 Effect of axial force on the first four natural frequencies with the fiber angle 60° in the flanges and web of a simply supported composite beam.

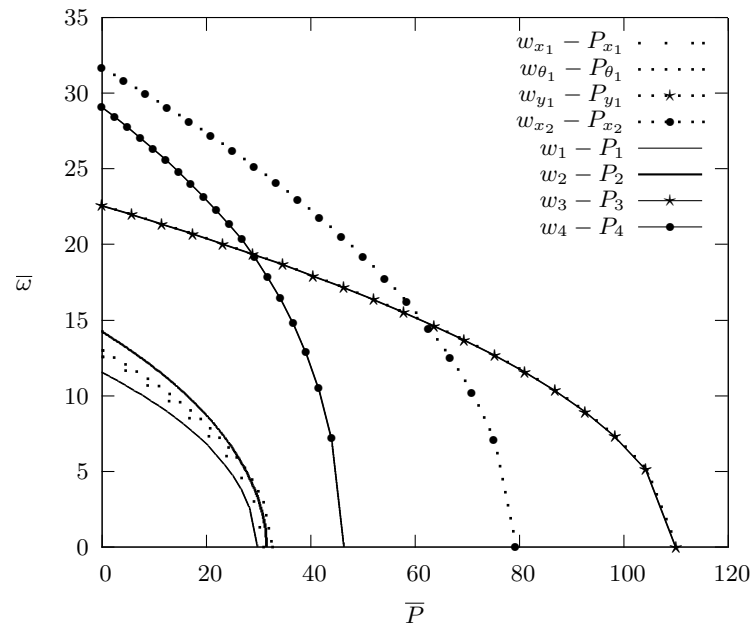


FIG. 8 Effect of axial force on the first four natural frequencies with the fiber angle 0° in the bottom flange of a clamped composite beam.

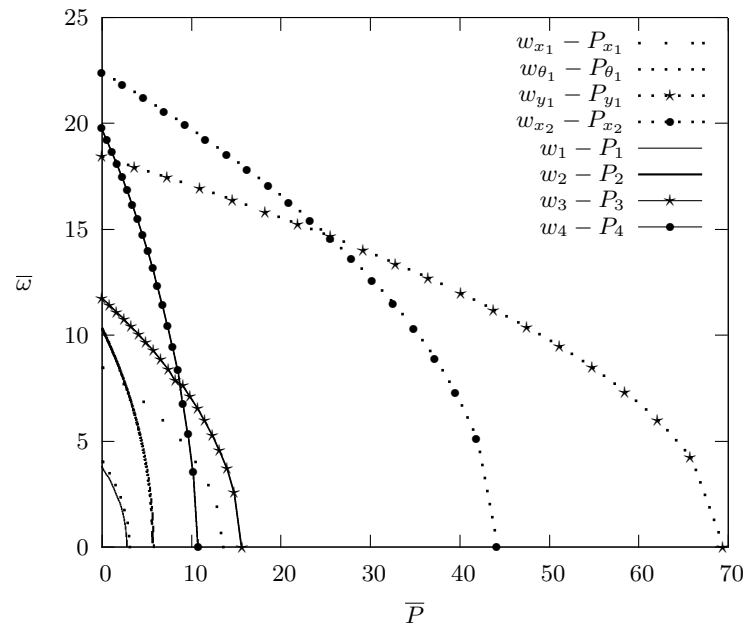


FIG. 9 Effect of axial force on the first four natural frequencies with the fiber angle 60° in the bottom flange of a clamped composite beam.

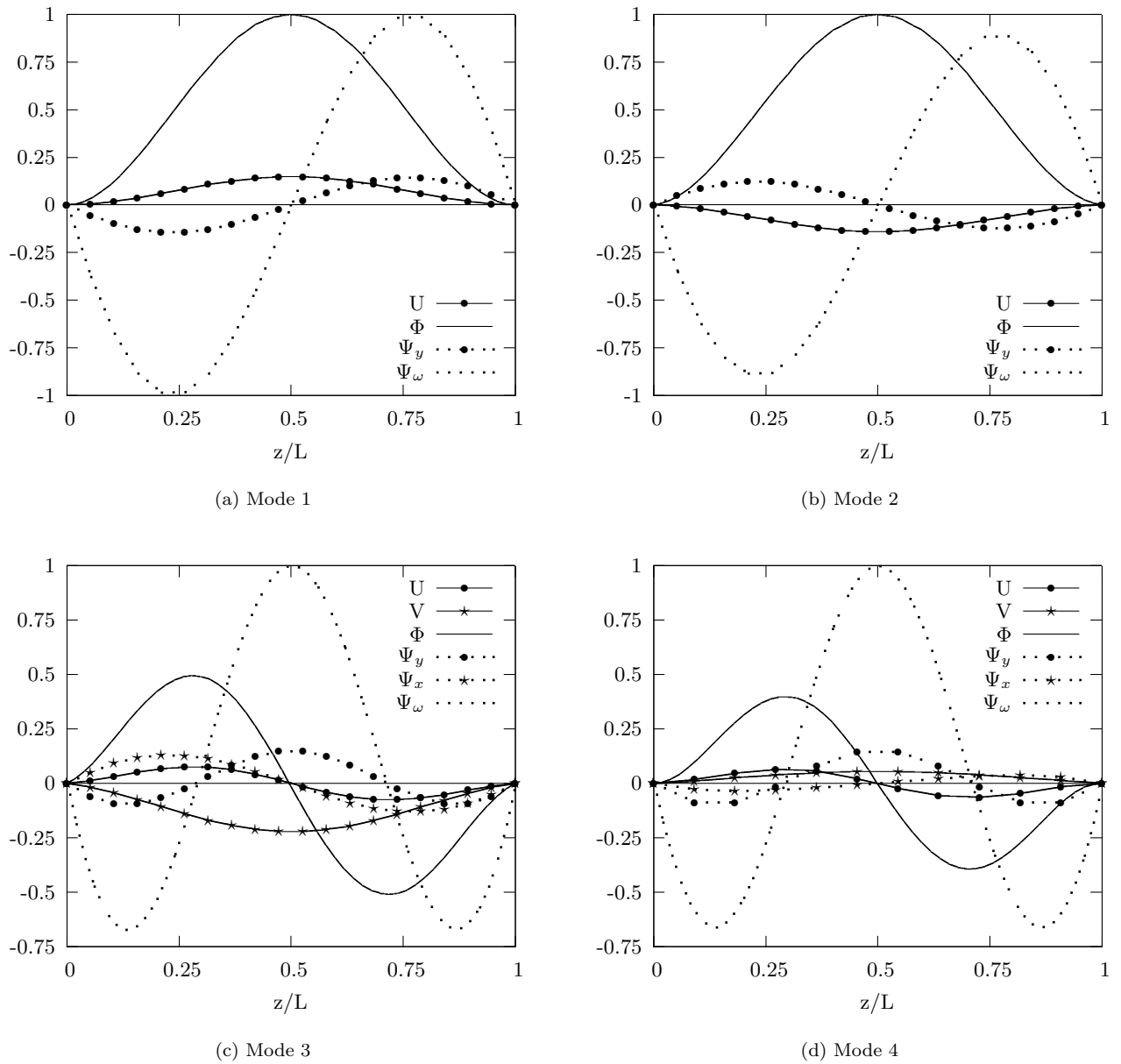


FIG. 10 The first four normal mode shapes of the flexural, torsional and corresponding shearing components with the fiber angle 30° in the bottom flange of a clamped composite beam under an axial compressive force ($\bar{P} = 0.5\bar{P}_{cr}$).

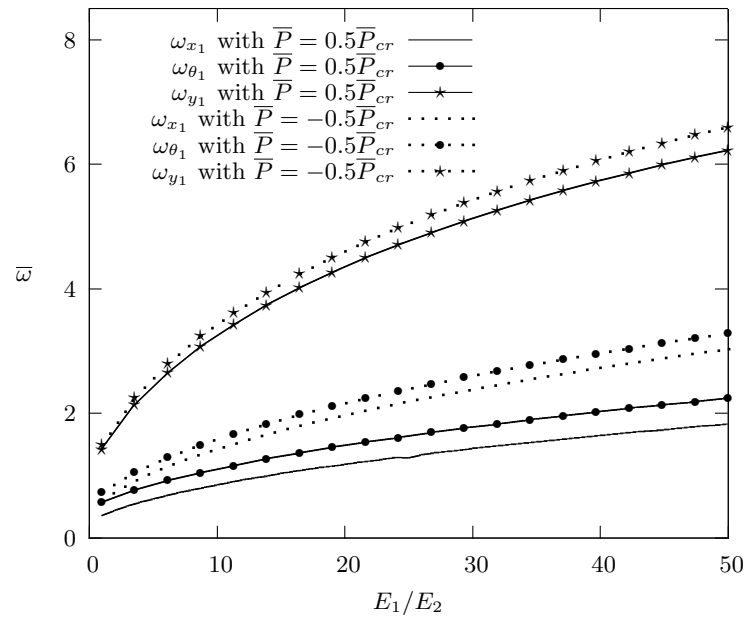


FIG. 11 Variation of the first three natural frequencies with respect to modulus ratio change of a cantilever composite beam under an axial compressive force ($\bar{P} = 0.5\bar{P}_{cr}$) and an axial tensile force ($\bar{P} = -0.5\bar{P}_{cr}$).